Dynamics of the reactions of O(1D) with CD3OH and CH3OD studied with time-resolved Fourier-transform IR spectroscopy

Chong-Kai Huang, Zhen-Feng Xu, Masakazu Nakajima, Hue M. T. Nguyen, M. C. Lin, Soji Tsuchiya, and Yuan-Pern Lee

Citation: The Journal of Chemical Physics **137**, 164307 (2012); doi: 10.1063/1.4759619
View online: http://dx.doi.org/10.1063/1.4759619
View Table of Contents: http://scitation.aip.org/content/aip/journal/jcp/137/16?ver=pdfcov
Published by the AIP Publishing

Dynamics of the reactions of O(^{1}D) with CD_3OH and CH_3OD studied with time-resolved Fourier-transform IR spectroscopy

Chong-Kai Huang,[1] Zhen-Feng Xu,[2] Masakazu Nakajima,[1,a)] Hue M. T. Nguyen,[3] M. C. Lin,[1,2,b)] Soji Tsuchiya,[1,b),c)] and Yuan-Pern Lee[1,4,b)]
[1]*Department of Applied Chemistry and Institute of Molecular Science, National Chiao Tung University, Hsinchu 30010, Taiwan*
[2]*Department of Chemistry, Emory University, Atlanta, Georgia 30322, USA*
[3]*Department of Physical Chemistry, Hanoi University of Technology, Hanoi, Vietnam*
[4]*Institute of Atomic and Molecular Sciences, Academia Sinica, Taipei 10617, Taiwan*

(Received 16 August 2012; accepted 4 October 2012; published online 24 October 2012)

We investigated the reactivity of O(^{1}D) towards two types of hydrogen atoms in CH_3OH. The reaction was initiated on irradiation of a flowing mixture of O_3 and CD_3OH or CH_3OD at 248 nm. Relative vibration-rotational populations of OH and OD ($1 \leq v \leq 4$) states were determined from their infrared emission recorded with a step-scan time-resolved Fourier-transform spectrometer. In O(^{1}D) + CD_3OH, the rotational distribution of OD is nearly Boltzmann, whereas that of OH is bimodal; the product ratio [OH]/[OD] is 1.56 ± 0.36. In O(^{1}D) + CH_3OD, the rotational distribution of OH is nearly Boltzmann, whereas that of OD is bimodal; the product ratio [OH]/[OD] is 0.59 ± 0.14. Quantum-chemical calculations of the potential energy and microcanonical rate coefficients of various channels indicate that the abstraction channels are unimportant and O(^{1}D) inserts into the C−H and O−H bonds of CH_3OH to form $HOCH_2OH$ and CH_3OOH, respectively. The observed three channels of OH are consistent with those produced via decomposition of the newly formed OH or the original OH moiety in $HOCH_2OH$ or decomposition of CH_3OOH. The former decomposition channel of $HOCH_2OH$ produces vibrationally more excited OH because of incomplete intramolecular vibrational relaxation, and decomposition of CH_3COOH produces OH with greater rotational excitation, likely due to a large torque angle during dissociation. The predicted [OH]/[OD] ratios are 1.31 and 0.61 for O(^{1}D) + CD_3OH and CH_3OD, respectively, at collision energy of 26 kJ mol^{-1}, in satisfactory agreement with the experimental results. These predicted product ratios vary weakly with collision energy. © *2012 American Institute of Physics*. [http://dx.doi.org/10.1063/1.4759619]

I. INTRODUCTION

The reactions of electronically excited oxygen atom O(^{1}D) with hydrocarbons have been the focus of many investigations concerned with atmospheric chemistry. For the simplest system, the reaction of O(^{1}D) + CH_4, several reaction channels that yield products, such as CH_3 + OH, H_2COH/CH_3O + H, and $H_2CO/HCOH$ + H_2, have been reported.[1] According to experiments with crossed molecular beams, the branching ratios of these three product channels are ~77%, 18%, and 5%, respectively.[1] A significant proportion of the product OH scattered in the forward and backward directions from the O(^{1}D) beam, indicating that the abstraction channel is important in the channel of OH formation. The observations of non-statistical vibration-rotational distributions of OH (Refs. 2–8) and CH_3 (Refs. 9 and 10) indicate that they are produced via a path with the lifetime of intermediate $CH_3OH^\dagger$ too small to complete the intramolecular vibrational relaxation (IVR).[11,12] The H products are noticeably scattered backward, whereas the H_2 products exhibit an isotropic angular distribution; the latter likely arises through a long-lived insertion intermediate. Direct information on the lifetime of the intermediate was given by half-collision experiments through the UV photodissociation of the O_3–CH_4 van der Waals complex;[13] the largest OH formation interval, 5.4 ps, corresponds to the reaction of the intermediate of which the internal energies are randomized statistically, whereas the smallest formation interval, 0.2 ps, corresponds to direct abstraction.

The potential-energy surface (PES) of the O(^{1}D)+CH_4 reaction calculated at a higher level indicates that the path of minimum energy follows a barrierless insertion of O(^{1}D) into the C−H bond to form intermediate CH_3OH and a direct abstraction path through a nearly collinear O−H−C geometry.[14–16] An additional abstraction path with a small barrier might occur on the electronically excited 2 ^{1}A surface. Based on this PES, quasiclassical trajectory calculations assuming the CH_3 group to act as a pseudoatom depict an internal distribution of OH in agreement with the experimental observations.[8,17]

In the reaction of O(^{1}D) with species that possess two types of H atoms, such as methanol (CH_3OH), the reaction paths are expected to be more complicated than those of O(^{1}D) + CH_4. O(^{1}D) might insert into either the C−H or the

a)Present address: Department of Basic Science, University of Tokyo, Komaba 3-8-1, Meguro-ku, Tokyo, 153-8902, Japan.
b)Authors to whom correspondence should be addressed. Electronic addresses: chemmcl@emory.edu, tsuchis@sepia.plala.or.jp, and yplee@mail.nctu.edu.tw.
c)Present address: Research Institute of Science and Engineering, Waseda University, Ookubo, Shinjuku-ku, Tokyo 169-8555, Japan.

O−H bond, or abstract a H atom directly from the CH_3 or OH moiety of CH_3OH. Goldstein and Wiesenfeld reacted $O(^1D)$ with partially deuterated methanol CH_3OD and CD_3OH and determined product ratios of [OH]/[OD] from the laser-induced fluorescence (LIF) of OH.[18] These authors reported that ~70% OH product arises from the hydroxyl site, whereas the reactions of $O(^1D)$ with the methyl group account for the remaining OH product. This result is in accord with the rate coefficient of the reaction $O(^1D) + CH_3OH$ reported as 5.1×10^{-10} $cm^3\,molecule^{-1}\,s^{-1}$,[19] which is much greater than the value $(1.5 \pm 0.4) \times 10^{-10}$ $cm^3\,molecule^{-1}\,s^{-1}$ for the reaction of $O(^1D) + CH_4$.[20] The greater rate coefficient for the reaction of $O(^1D)$ with CH_3OH than with CH_4 was attributed to an increased reactivity of $O(^1D)$ towards the OH moiety of CH_3OH. Goldstein and Wiesenfeld also determined the vibrational populations of $OH(v = 0, 1)$ and $OD(v = 0-2)$ and concluded that an attack on the methyl moiety of methanol generates greater vibrational excitation of hydroxyl radicals than that from attack on the hydroxyl moiety. In these experiments, vibrational states of the product OH or OD beyond $v = 1$ or 2, respectively, were unreported due to the limitation of the LIF method associated with the predissociation of the electronically excited state.[18] Moreover, their reaction system included a buffer gas (He at 10 Torr), precluding information on the rotational distribution of OH; the vibrational distribution of OH might also be affected by collisional relaxation under such conditions. Matsumi *et al.* detected H atoms with the LIF method and determined a quantum yield of 0.18 for production of H atom in the reaction of $O(^1D) + CH_3OH$.[19] These authors reported that $[H]/[D] = 0.26 \pm 0.03$ and 7.1 ± 0.8 for the reaction of $O(^1D)$ with CD_3OH and CH_3OD, respectively. To explain the selectivity in the formation of product H, two possible mechanisms were considered: (1) insertion of an O atom into the C−H bond is followed by preferential breaking of the new O−H bond because of incomplete IVR in the reaction intermediate, and (2) cleavage of the C−H bond is more likely to occur than of the O−H bond of the reaction intermediate $HOCH_2OH$ because the dissociation energy of the former is smaller than of the latter. Despite all these preceding works, information on the rotational distribution and a more complete vibrational distribution of OH is lacking.

Here, we report our observations of rotationally resolved infrared (IR) emission spectra of OH and OD that were produced from the reaction of $O(^1D)$ with CH_3OD and CD_3OH. One advantage of IR emission spectroscopy is the ability to monitor OH and OD in vibration-rotational levels greater than $v = 2$, which are difficult to detect with the LIF method because of predissociation. In addition to the rotational distributions of OH and OD, we determined also the ratio of [OH]/[OD]. We calculated quantum-chemically the PES of various reaction channels and predicted accordingly the branching ratios to assist the interpretation of experimental data.

II. EXPERIMENTS

The apparatus employed to obtain time-resolved emission spectra is based on a step-scan Fourier-transform spectrometer (FTS) that was described previously;[21–23] only a brief summary appears here. For experiments on $O(^1D)$ + methanol, ozone (O_3), and methanol were injected separately into the reaction chamber. A telescope mildly focused the photolysis beam from a KrF laser (248 nm, 19 Hz) to an area $\sim 12 \times 10$ mm^2 at the reaction center to yield a fluence of ~ 53 mJ cm^{-2}; this laser beam decomposed O_3 to form $O(^1D)$. IR emission was collected with two Welsh mirrors (focal length 10 cm), directed into the step-scan FTS, and detected with an InSb detector (Kolmar Technologies) equipped with a preamplifier (rise time 0.34 μs and responsivity 3.2×10^6 $V\,W^{-1}$). The transient signal from the InSb detector was further amplified 20 times with a voltage amplifier (Stanford Research Systems, model 560, bandwidth 1 MHz) before being digitized with an external data-acquisition board (12-bit) at 25-ns resolution. Data were typically averaged over 60 laser pulses at each scan step; 4569 scan steps were performed to yield an interferogram resulting in spectra of resolution 0.8 cm^{-1} in a spectral range of 3800–2170 cm^{-1} to cover the emission of OH and OD. For the reaction of $O(^1D) + CH_3OH$, 3473 scan steps were performed to yield an interferogram resulting in spectra of resolution 0.5 cm^{-1} in a spectral range of 3650–2950 cm^{-1} to cover emission of OH. To increase further the ratio of signal to noise, five spectra recorded under similar conditions were averaged. The temporal response function of the instrument was determined with a pulsed IR laser beam, as described in Ref. 24. The temporal response period of the detection system is approximately 1 μs, determined with an IR laser emission. The spectral response function was calibrated with a black-body radiation source.

To decrease the collision quenching of OH and OD, a minimal pressure yielding satisfactory signals was used: $P_{O_3} = 0.018-0.022$ Torr, $P_{CD_3OH} = P_{CH_3OD} \cong 0.105$ Torr. Flow rates were $F_{O_3} = 0.7-1.0$ sccm, $F_{CD_3OH} = F_{CH_3OD} = 3.9-4.5$ sccm, in which sccm denotes $cm^3\,min^{-1}$ under standard conditions (1 atm and 298.15 K). Approximately 60% of O_3 was dissociated upon irradiation at 248 nm according to the reported absorption cross section of $\sim 1.1 \times 10^{-17}$ $cm^2\,molecule^{-1}$ and $O(^1D)$ quantum yield of $\sim 0.90 \pm 0.05$ for O_3 at 248 nm[25,26] and the laser fluence used. The depletion of O_3 in the flowing system after each laser pulse was modest, as was confirmed by the negligible variation of the signal intensity when we varied the repetition rate of the photolysis laser from 19 Hz to 30 Hz.

CH_3OH (99.9%, Mallinckrodt), CD_3OH (isotopic purity 99.5%, Cambridge Isotope Laboratories), and CH_3OD (isotopic purity 99%, Cambridge Isotope Laboratories) were employed without further purification. For experiments with CH_3OD, the reaction chamber was heated to 373 K under vacuum followed by passivation with D_2O (10 Torr) at 298 K for 1 h. After evacuation, the system was filled with D_2O (10 Torr) overnight and was treated with passivation and evacuation three times before each experiment. O_3 was produced from O_2 (Scott Specialty Gases, 99.995%) with an ozone generator (Polymetrics, Model T-408) and stored over silica gel at 196 K. The partial pressure of O_3 was determined from the absorption of Hg emission at 254 nm in a cell of length 7.0 cm; the absorption cross section of $\sim 1.1 \times 10^{-17}$ cm^2 for O_3 at 254 nm was used.[26]

III. COMPUTATIONS

A. Potential-energy surfaces and branching ratios

The geometries of reactants, products, intermediates, and transition states on the PES of the $O(^1D) + CH_3OH$ reaction were optimized with the B3LYP/aug-cc-pVTZ density-functional theory (DFT).[27–30] The vibrational wavenumbers were calculated at this level to characterize local minima and the transition state and to correct for the zero-point energy. To obtain reliable energies and predictions of rate coefficients, we calculated single-point energies at the CCSD(T)/aug-cc-pVTZ[31,32] level based on the structures predicted with B3LYP/aug-cc-pVTZ, expressed as CCSD(T)//B3LYP/aug-cc-pVTZ. For the abstraction channels, whose transition states could not be found by the DFT method, we calculated energies with the MRCI(8,8)//CAS(10,10)/6-311+G(3df,2p) methods.[33,34] Calculations of the intrinsic reaction coordinate[35] were performed to connect each transition state with the designated reactants and products. All calculations of electronic structure were performed with the GAUSSIAN 03 (Ref. 36) and MOLPRO programs.[37]

The minimum energy path (MEP) representing a barrierless insertion or association process was obtained by calculating the potential energy curve at the CASPT2(8,8)/6-311+G(3*df*,2*p*)//CAS(8,8)/6-311+G(3*df*,2*p*) level of theory along its reaction coordinate: O···H (for C−H or O−H abstraction), O···C (for C−H insertion), or O···O (for O−H insertion) from its equilibrium separation to ∼5 Å at step size of 0.1 Å and with other geometric parameters fully optimized. The MEP was fitted to the Morse potential function $E(R) = D_e\ [1 - \exp(-\beta(R - R_e))]^2$ and employed to approximate the variational transition state in calculations of rate coefficients. In the above equation, R is the reaction coordinate (i.e., the distance for O···H, O···C, or O···O), D_e is the bond dissociation energy excluding zero-point energy, β is an exponential factor, and R_e is the equilibrium value of R of an insertion product or an association intermediate. The numbers of states for the tight transition states are evaluated according to the rigid-rotor harmonic-oscillator approximation. The lower vibrational modes in the transition states were treated as classical one-dimensional free rotors. For those paths involving hydrogen atom transfer, Eckart tunneling effects[38] were taken into account in the rate coefficient calculations. The employment of the statistical theory in these rate coefficient calculations implies rapid energy redistributions among all internal degrees of freedom.

The rate coefficients for production of H, D, OH, OD, H_2O, HOD, and D_2O were predicted according to the following method. We employed the variational transition-state theory for the direct abstraction reactions and the variational Rice-Ramsperger-Kassel-Marcus (RRKM) theory[39–42] with Eckart tunneling correction for the insertion/decomposition processes using the VARIFLEX code[43] by solving the master equation for the formation and removal of the excited intermediates ($HOCH_2OH^*$ or CH_3OOH^*). The removal processes include collisional deactivation and various decomposition reactions. Thus the effects of pressure, temperature, isotopic substitution as well as the kinetic energy carried by the $O(^1D)$ atom on the formation of individual products can be reliably examined. To obtain rate coefficients at excess energy E, the energies of all transition states and intermediates involved in the insertion/decomposition paths were increased by the amount because the excess translational energy can be quantitatively injected into the excited adducts ($HOCH_2OH^*$ or CH_3OOH^*) before their isomerization and fragmentation.

The energy increment was fixed at 10 cm^{-1} in all calculations of sums and densities of states using the modified Beyer-Swinehart algorithm.[44] For the decomposition with loose transition states, the potential energy paths are approximated with three parts.[45] The first part is represented with a Morse function. The second part corresponds to the internal degrees of freedom of the separate fragments and is assumed to be the same as the normal-mode vibrations of the fragments. The third part is the potential energy for the transitional modes, which is described in terms of a set of internal angles with a sum of products of sinusoidal functions. In the RRKM calculations, the L-J values for $HOCH_2OH$ and CH_3OOH, were approximated with $\sigma = 4.317$ Å and $\varepsilon/\kappa = 450.2$ K.[46]

B. Einstein *A* coefficients for vibration-rotational transitions of OH/OD

The rotational states of the OH radical, an open-shell molecule with ground state $X\ ^2\Pi$, consist of two spin sublevels F_1 and F_2 corresponding to $J = N + 1/2$ and $J = N - 1/2$, respectively; each J level splits into e and f states through the Λ-doubling. Because the spin uncoupling depends on J, OH is intermediate between Hund's cases (a) and (b). For the assignment of our emission spectra of OH, we referred to the high-resolution data and molecular parameters of OH[47,48] and OD.[49–51]

A diatomic hydride molecule OH has a large rotational constant and the large rotational constant causes a large extent of centrifugal distortion effect on the radial part of the wavefunction that changes significantly the magnitude of the transition dipole moment (the Herman-Wallis effect);[52] the Einstein A coefficients must consequently be evaluated for respective vibration-rotational transitions. Nelson *et al.* derived the electric dipole-moment function of OH from observations of the relative intensities of vibration-rotational transitions of OH.[53] Using this function, they calculated the Einstein A coefficients of vibration-rotational transitions according to

$$A(v'J'F' \rightarrow v''J''F'') = \frac{16\pi^3\nu^3}{3\varepsilon_0 hc^3}|\langle v'J'F'|\mu(r)|v''J''F''\rangle|^2, \quad (1)$$

in which $\mu(r)$ is the dipole-moment function and $|v'J'F'\rangle$ is the eigenfunction of the vibration-rotational state of OH in which the Λ-type splitting is disregarded. To estimate the population distribution of OH in this work, we employed a table of the Einstein A coefficients reported by Holzclaw *et al.*[54] who calculated the transition dipole moment according to the dipole-moment functions reported by Nelson *et al.*[53] from the numerical solution of the Schrödinger equation in which the RKR potential was introduced.

Since there is no available data for the Einstein A coefficients of the OD Meinel bands, we calculated them following the method described by Nelson *et al.*[55] The details of our calculation and the resultant Einstein A coefficients of OD are available in the supplementary material.[56] The transition strength for various J' values of the R-branches of OD, as also seen in the case of OH, is significantly smaller than the corresponding values of the P-branches because of a negative contribution of the vibration-rotational coupling to the transition dipole moment. We therefore analyzed only the P-branch transitions with spin-sublevel transitions of $F_1 \rightarrow F_1$ and $F_2 \rightarrow F_2$, which are denoted P_1 and P_2, respectively.

IV. RESULTS AND DISCUSSION

A. IR emission from the O(¹D) + CD_3OH system

Figure 1 shows the time-resolved emission spectra in the spectral regions 2800–3700 and 2160−2650 cm^{-1} recorded at 1-μs intervals for the first 3 μs upon irradiation at 248 nm of a flowing mixture of O_3/CD_3OH (1/5.3, 0.125 Torr); O(¹D) was generated on photolysis of O_3 to react with CD_3OH. Sharp lines in two groups located in the regions 2800–3700 cm^{-1} and 2160–2600 cm^{-1} are identified, together with two broad feature covering the regions 2160−2350 cm^{-1} with a maximum near 2200 cm^{-1}. The first and second groups of sharp lines are readily assigned to the $\Delta v = -1$ transitions of OH and OD radicals, respectively, and the observed broad feature is likely co-products of OH or OD. Because it is difficult to identify positively the carrier of this feature from the available information, we concentrate on the analysis of spectral lines of OH and OD.

The intensities of emission lines of OH and OD rise towards their maxima ~2 μs after irradiation of the flowing sample at 248 nm. Because the initial concentration of CD_3OH, ~3.4 × 10^{15} molecule cm^{-3}, is much greater than that of O(¹D), the condition of pseudo-first-order reaction is valid. The pseudo-first-order rate coefficient $k^I = 2 \times 10^6$ s^{-1}, in which the rate coefficient of O(¹D) + CH_3OH was reported by Matsumi *et al.*,[19] is in accord with the observed rise time for emission of OH or OD. For an improved ratio of signal to noise, we analyzed the distribution of internal states of OH or OD according to the emission spectra averaged over 0−5 μs, and corrected for the small rotational quenching effect, as described later.

The assignments of the observed lines to vibration-rotational transitions of OH and OD, indicated at the top part of Fig. 1, were made according to the high-resolution spectral data for OH (Refs. 47 and 48) and OD;[49–51] most lines are associated with transitions of P_1 ($F_1 \rightarrow F_1$) and P_2 ($F_2 \rightarrow F_2$) for $\Delta v = -1$ ($v = 1-3$). Lines associated with R_1, R_2, Q_1, and Q_2 transitions have much smaller intensity as J increases, consistent with the report by Nelson *et al.*[53,55] Most Λ doublet e and f lines are unresolved because the resolution was set at 0.8 cm^{-1} in these experiments. For $J' \geq 10.5$, the e/f splitting exceeds 1 cm^{-1}, resulting in broadened lines or partially resolved lines. In this experiment, we made no attempt to separate the populations of the e and f transitions, but used the total population for each vibration-rotational

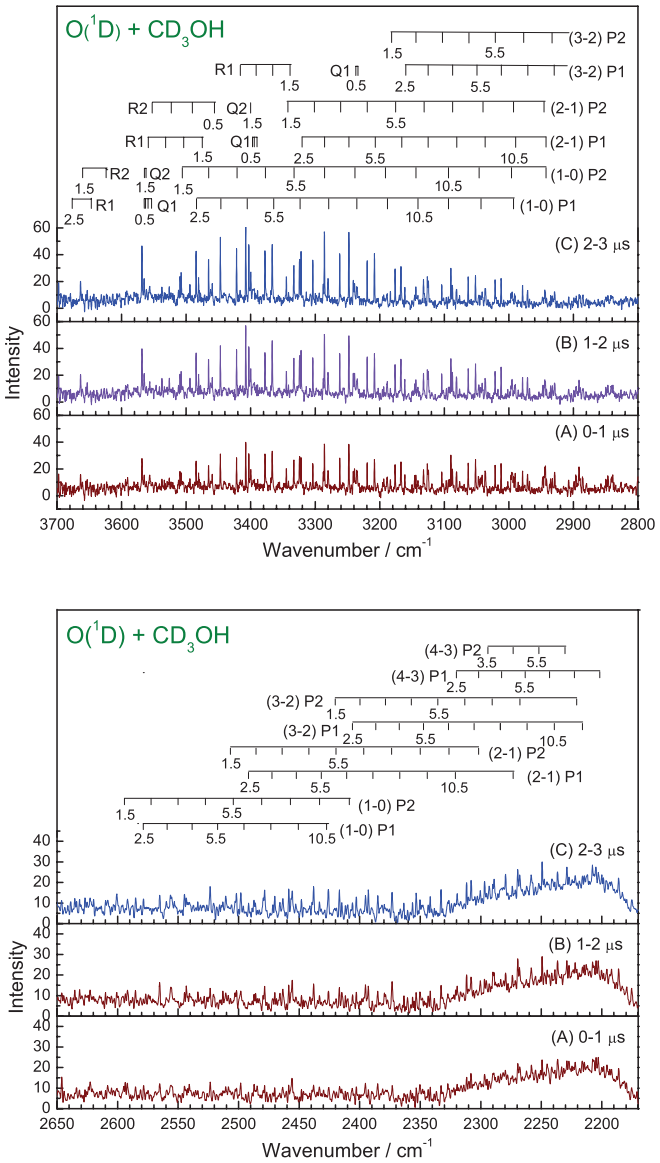

FIG. 1. Observed IR emission spectra of the reaction system O(¹D) + CD_3OH recorded at 1-μs intervals. The spectral resolution is 0.8 cm^{-1}. Partial pressures of O_3 and CD_3OH are 0.018−0.022 and 0.104−0.106 Torr, respectively. The assignments of vibration-rotational transitions are shown as stick diagrams for OH and OD, respectively; the numbers correspond to J''.

transition. To analyze these observed lines, we assumed a Gaussian shape for each line and performed curve fitting on each line, including overlapped lines.

To improve the ratio of signal to noise in these experiments, the micropopulation was determined from spectral lines integrated for 0−5 μs after photoirradiation. Each vibration-rotational line in the P branch was normalized with the instrument spectral-response function, and divided by its respective Einstein coefficient to yield a relative population $P_v(v', J', F')$. In Fig. 2, the logarithm of the micropopulation in a rotational state (v', J', F'), defined as $P_v(v', J', F')/(2J' + 1)$, is plotted as a function of the rotational energy that is defined as the average of the e and f term values from which the vibrational term value is subtracted. The micropopulations of the F_1 and F_2 components are similar, as indicated in

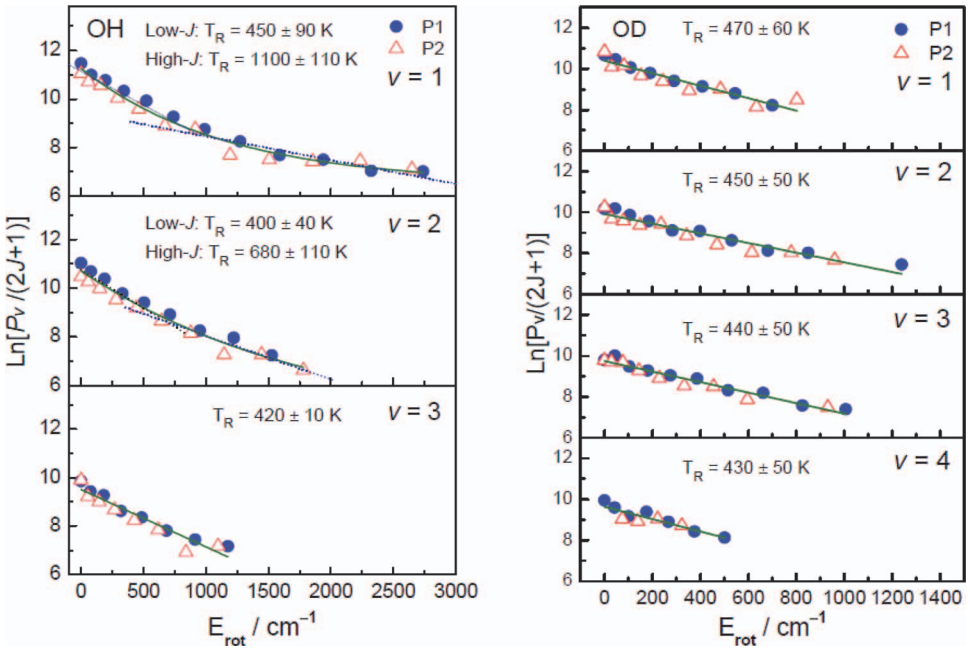

FIG. 2. Semilogarithmic plots of the rotational populations of OH and OD as a function of the rotational energy in respective vibrational levels formed from the $O(^1D)+CD_3OH$ reaction. Average period is 0−5 μs.

Fig. 2 for values derived from P_1 (shown as blue dots) and P_2 (red triangles) branches.

As shown clearly in Fig. 2, the rotational distribution of OH is not singly exponential, whereas that of OD is nearly exponential (Boltzmann). Average rotational energies for each vibrational level of OH and OD, $E_r(v)$, were obtained on summing the product of rotational level energy and normalized population over all observed rotational levels. The average rotational energy E_r was derived on multiplying the observed $E_r(v)$ with the respective vibrational population, to be discussed later. The average rotational energies E_r of OH and OD are thus calculated to be 11 ± 3 and 5 ± 1 kJ mol^{-1}, respectively; E_r of OD is much smaller than that of OH.

For OD, we derived rotational temperatures (T_R) of 470 ± 60, 450 ± 50, 440 ± 50, and 430 ± 40 K for $v = 1-4$, respectively. Because the rotational distributions of OH($v = 1$) and OH($v = 2$) are non-Boltzmann, we fitted them with biexponential functions and derived the rotational temperatures 450 ± 90 K ($v = 1$) and 400 ± 40 K ($v = 2$) of the low-J component and 1100 ± 110 K ($v = 1$) and 680 ± 110 K ($v = 2$) of the high-J component. For OH($v = 3$), we could fit only a rotational temperature of 420 ± 10 K because of the limited levels observed. The population ratio of the high-J component to the low-J component is ~35/65. Because the spectra were integrated for 0−5 μs, the rotational temperatures reflect the average value in this period.

To derive the nascent rotational energy, we estimated the quenching effects by measuring the rotational temperature as a function of time. By integrating the observed lines at 1-μs intervals, we determined the rotational temperature of OD and the high-J and low-J components of OH as a function of time. The rotational temperatures of OD(v) determined at 1-μs intervals are shown in Fig. 3. The nascent rotational temperatures of 570 ± 190 K, 560 ± 100 K, and 560 ± 60 K were derived for OD($v = 1-3$), respectively, after a short extrapolation to $t = 0$. According to this measurement of the rotational quenching, we estimated that the nascent rotational temperature should be multiplied by 1.2 ± 0.1 for OD, compared with those determined for 0−5 μs. Using a similar method, we

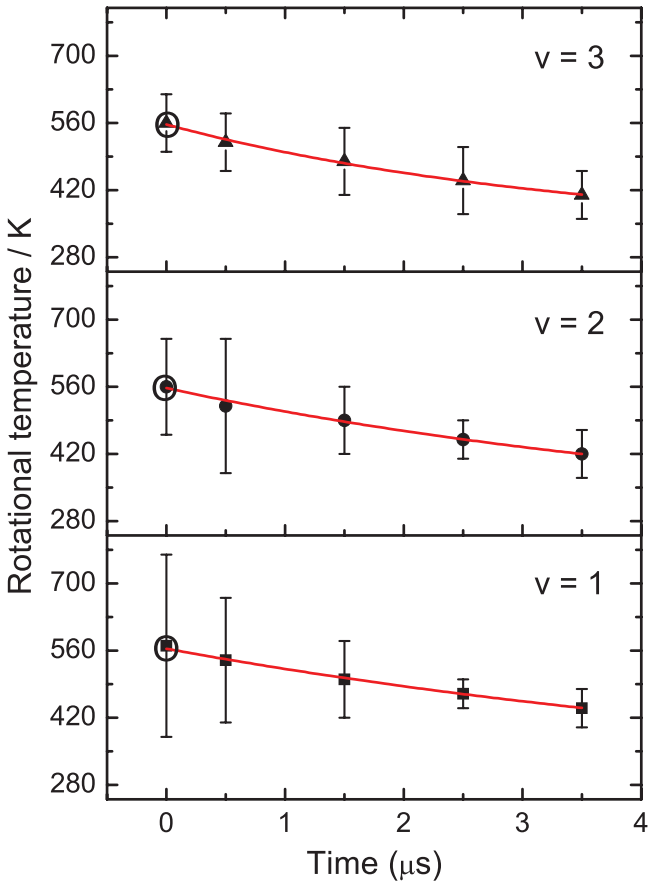

FIG. 3. Plot of rotational temperature of OD ($v = 1-3$) as a function of time. The data extrapolated to $t = 0$ are indicated with o.

TABLE I. Summary of experimental results for reactions $O(^1D)$ + CH_3OD/CD_3OH.

	$O(^1D) + CD_3OH$[a]		$O(^1D) + CH_3OD$[a]	
Products rotation	OH bimodal	OD Boltzmann	OH Boltzmann	OD bimodal
T_R ($v = 1$) (K)	450 ± 90	470 ± 60	410 ± 50	250 ± 20
	1100 ± 110			990 ± 30
T_R ($v = 2$) (K)	400 ± 40	450 ± 50	440 ± 70	280 ± 30
	680 ± 110			920 ± 40
T_R ($v = 3$) (K)	420 ± 10	440 ± 50	410 ± 50	350 ± 20
T_R ($v = 4$) (K)		430 ± 50		
E_r (kJ mol^{-1})	11 ± 3	5 ± 1	5 ± 1	9 ± 2
	(12 ± 4)[b]	(6 ± 2)[b]	(6 ± 2)[b]	(10 ± 3)[b]
E_v (kJ mol^{-1})	28 ± 6	43 ± 8	65 ± 15	27 ± 5
[OH]/[OD]	1.56 ± 0.36		0.59 ± 0.14	

[a]Unless otherwise noted, the data are derived from spectra integrated over 0–5 μs after photolysis of O_3.

[b]Estimated nascent average rotational energy. For bimodal distributions, average energies for the high-J and low-J components are 18 ± 5 and 6 ± 2 for the reaction $O(^1D) + CD_3OH$ and 14 ± 3 and 5 ± 2 for the reaction $O(^1D) + CH_3OD$. The population ratio of these two components are ~50/50.

estimated that the nascent rotational temperature should be multiplied by 1.2 ± 0.1 for the low-J component of OH, and 1.8 ± 0.3 and 2.1 ± 0.4 for the high-J component of OH ($v = 1$ and 2), respectively, compared with those determined for 0–5 μs. We hence estimate the average nascent rotational energies to be 6 ± 2 kJ mol^{-1} for OD and 18 ± 5 and 6 ± 2 kJ mol^{-1}, respectively, for the high-J and low-J components of OH; the energy of the high-J component is less accurate because of the large factor of correction. After correction for quenching, the population ratio of the nascent high-J component to the low-J component is ~50/50; the nascent average rotational energy of OH is thus 12 ± 4 kJ mol^{-1}, as listed in Table I.

The relative vibrational populations were derived on counting levels up to the observed maximal J' values in each vibrational level, $\Sigma_{J',F'} P(v', J', F')$. We normalized the values of $\Sigma_{J',F'} P(v', J', F')$ associated with each vibrational state to yield a relative vibrational population $(v' = 1) : (v' = 2) : (v' = 3) = 54.8 : 33.7 : 11.5$ for OH and $(v' = 1) : (v' = 2) : (v' = 3) : (v' = 4) = 34.9 : 28.6 : 22.7 : 13.8$ for OD.

In our IR chemiluminescence experiments, it is impossible to obtain directly information about the population of the vibrational ground state; the population of $v' = 0$ was hence estimated on extrapolation from the populations of levels $v' \geq 1$ assuming a Boltzmann distribution. The populations of $v' = 0$ relative to $v' = 1$ were thus derived to be 2.4 ± 0.3 and 1.5 ± 0.2 for OH and OD, respectively. After renormalizing, we derived vibrational distributions of OH as $(v' = 0) : (v' = 1) : (v' = 2) : (v' = 3) = 56.8 : 23.7 : 14.6 : 4.9$ and of OD as $(v' = 0) : (v' = 1) : (v' = 2) : (v' = 3) : (v' = 4) = 34.1 : 23.0 : 18.9 : 14.9 : 9.1$. These vibrational distributions of OH and OD are shown in Fig. 4(a).

The observed ratios of total populations of OH ($v = 1$–3) and OD ($v = 1$–4) are derived to be ~50/50. When we include the estimated populations for the $v = 0$ levels of OH and OD, the total ratios of populations of OH ($v = 0$–3) and OD ($v = 0$–4) are derived to be (61 ± 9)/(39 ± 9) = 1.56 ± 0.36. This ratio is slightly smaller than, but within the error limit of, the ratio (71 ± 12)/(29± 12) = 2.45 ± 1.01 determined from OH ($v = 0$, 1) and OD ($v = 0$–2) by Goldstein and Wiesenfeld.[18] The discrepancy is partly due to the fact that their observations were limited to populations in small vibrational levels of OH and OD. As seen from Fig. 4(a), the populations of OD ($v > 2$) contribute much more significantly than those of OH ($v \geq 2$).

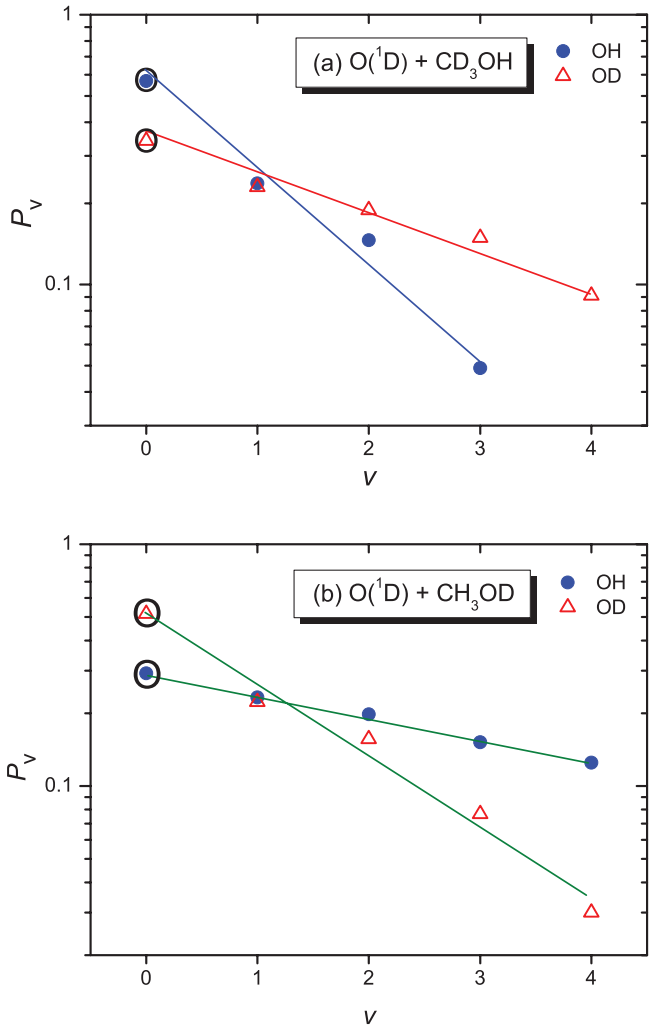

FIG. 4. Relative vibrational populations of OH and OD produced from the $O(^1D) + CD_3OH$ reaction (a) and $O(^1D) + CH_3OD$ reaction (b) as a function of vibrational quantum number v. Populations in $v = 0$ are derived by extrapolation.

Using this distribution of vibrational populations, we calculated the average vibrational energies of OH and OD to be 28 ± 6 and 43 ± 8 kJ mol^{-1}, respectively, as listed in Table I. The vibrational energy of OH is slightly smaller than that of OD; in contrast, the rotational energy of OH is greater than that of OD.

B. Infrared emission from the $O(^1D) + CH_3OD$ system

To discriminate the reaction sites of $O(^1D)$ towards the methyl and hydroxyl groups in methanol, we investigated also the reaction $O(^1D) + CH_3OD$. In the reaction of $O(^1D) + CH_3OD$, the channels that produce OH and OD correspond

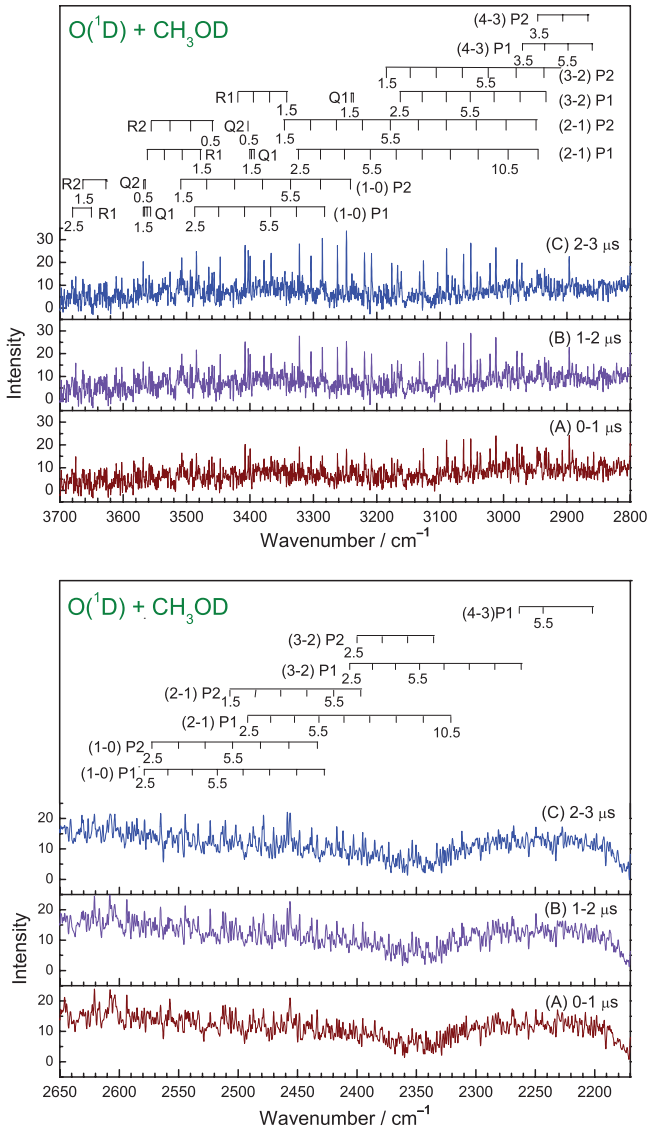

FIG. 5. Observed IR emission spectra of the reaction system $O(^1D)+CH_3OD$ recorded at 1-μs intervals. The spectral resolution is 0.8 cm^{-1}. Partial pressures of O_3 and CH_3OD are 0.018−0.022 and 0.104−0.106 Torr, respectively. The assignments of vibration-rotational transitions in P branches are given as stick diagrams for OH and OD, respectively; the numbers correspond to J''.

to channels that produce OD and OH, respectively, in the reaction of $O(^1D) + CD_3OH$.

The time-resolved IR emission spectra observed at 1-μs intervals from the $O(^1D) + CH_3OD$ system are shown in Fig. 5. Similar to the reaction of $O(^1D) + CD_3OH$, two groups of sharp lines located in regions of 3700−2800 and 2650−2160 cm^{-1} are assigned as the $\Delta v = -1$ vibration-rotational transitions of OH and OD, respectively. In addition, broad emission bands are evident in the regions of 3600−3200, 3100−2350, and 2350−2160 cm^{-1} that might have originated from the co-products of OH or OD, likely CH_2DO or CH_3O. Compared with the spectra of OH and OD in the reaction system of $O(^1D)+CD_3OH$, the line intensities are smaller for both OH and OD and the distributions of internal states differ. The relative rotational micropopulations of the respective vibrational states of OH and OD determined from the line intensities integrated for 0−5 μs are shown as a function of rotational energy in Fig. 6. The rotational distributions of OH are nearly singly exponential as in the case of OD produced from the reaction of $O(^1D) + CD_3OH$. In contrast, the rotational distributions of OD are biexponential, similar to those of OH from the reaction $O(^1D) + CD_3OH$. The result is in accord with the expectation for such isotopic substitutions. Following a method similar to that described in Sec. IV A, the average rotational energies of OH and OD for the period 0−5 μs are thus calculated to be 5 ± 1 and 9 ± 2 kJ mol^{-1}, respectively, as listed in Table I.

For OH, we derived rotational temperatures of 410 ± 50, 440 ± 70, and 410 ± 50 K for $v = 1-3$, respectively. We fitted the rotational distributions of OD($v = 1$) and OD($v = 2$) with biexponential functions and derived the rotational temperatures 250 ± 20 K ($v = 1$) and 280 ± 20 K ($v = 2$) of the low-J component and 990 ± 320 K ($v = 1$) and 920 ± 400 K ($v = 2$) of the high-J component. For OD($v = 3$), we could fit only a rotational temperature of 350 ± 20 K for the low-J component because of the limited levels observed. The ratio of the high-J component to the low-J component of OD is ∼48/52. Because the spectra were integrated for 0−5 μs, the rotational temperatures reflect the average value during this period.

According to measurements of rotational quenching we estimated that the nascent rotational temperature should be multiplied by 1.3 ± 0.2 for OH, 1.2 ± 0.2 for the low-J component of OD, and 1.3 ± 0.3 for the high-J component of OD, respectively. We hence estimate the average nascent rotational energy to be 6 ± 2 kJ mol^{-1} for OH, and 14 ± 3 and 5 ± 2 kJ mol^{-1}, respectively, for the high-J and low-J components of OD. After correction for quenching, the population ratio of the nascent high-J component to the low-J component is ∼50/50; the average rotational energy of OD is thus 10 ± 3 kJ mol^{-1}, as listed in Table I.

We normalized the values of $\Sigma_{J',F'} P(v', J', F')$ associated with each vibrational state to yield a relative vibrational population ($v' = 1$) : ($v' = 2$) : ($v' = 3$) : ($v' = 4$) = 32.8 : 28.0 : 21.5 : 17.7 for OH and ($v' = 1$) : ($v' = 2$) : ($v' = 3$) : ($v' = 4$) = 45.9 : 32.1 : 15.8 : 6.2 for OD. The population of $v' = 0$ is estimated on extrapolation from the populations of levels $v' \geq 1$ according to the Boltzmann distribution; the populations of $v' = 0$ relative to $v' = 1$ were thus derived to be 1.3 ± 0.2 and 2.3 ± 0.5 for OH and OD, respectively. After renormalizing, we derived the vibrational distributions of OH as ($v' = 0$) : ($v' = 1$) : ($v' = 2$) : ($v' = 3$) = 29.3 : 23.2 : 19.8 : 15.2 : 12.5 and of OD as ($v' = 0$) : ($v' = 1$) : ($v' = 2$) : ($v' = 3$) : ($v' = 4$) = 51.4 : 22.3 : 15.6 : 7.7 : 3.0. These vibrational distributions of OH and OD are shown in Fig. 4(b).

The observed ratios of total populations of OH ($v = 1-3$) and OD ($v = 1-4$) are derived to be 46/54. When we include the estimated populations for the $v = 0$ levels of OH and OD, the ratio of total populations of OH ($v = 0-3$) and OD ($v = 0-4$) become (37 ± 9)/(63 ± 9) = 0.59 ± 0.14. This ratio is slightly larger than the ratio (30± 6)/(70 ± 6) = 0.43 ± 0.09 reported by Goldstein and Wiesenfeld.[18] Part of the discrepancy arises because their observations are limited to populations in levels $v = 0$ and 1 of OH and OD. As seen from Fig. 4(b), the populations of OH ($v \geq 2$) contribute

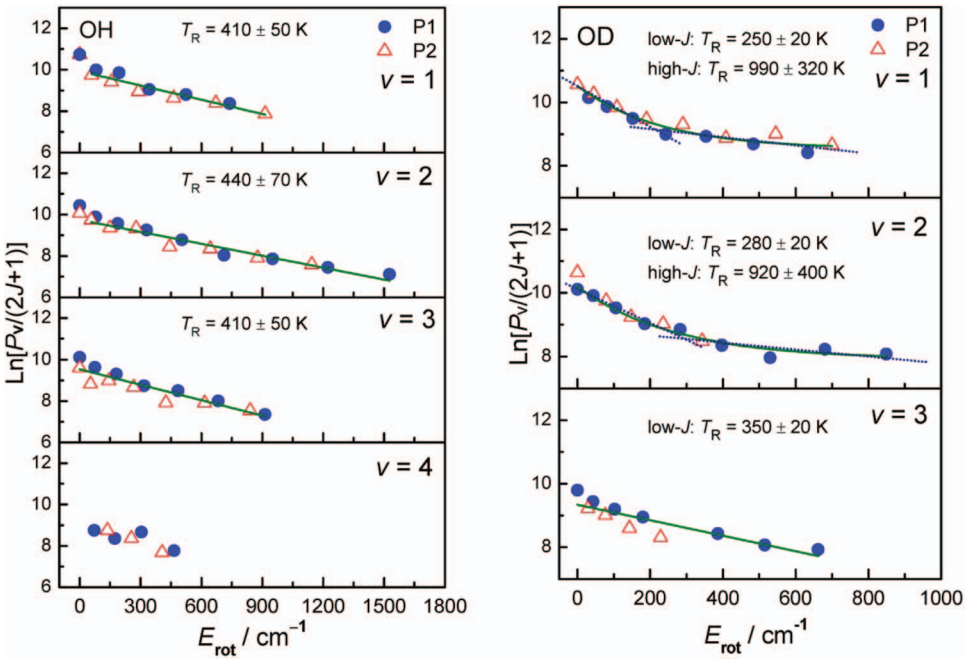

FIG. 6. Semilogarithmic plots of the rotational populations of OH and OD as a function of the rotational energy in respective vibrational levels formed from the O(^{1}D) + CH_3OD reaction. Average period is 0−5 μs.

much more significantly than that of OD ($v \geq 2$). The determined ratio [OH]/[OD] = 0.59 ± 0.14 in O(^{1}D) + CH_3OD is, notably, practically the same as the inverse of the value [OH]/[OD] = 1.56 ± 0.36 observed for O(^{1}D) + CD_3OH.

Using this distribution of vibrational populations, we calculated the average vibrational energies of OH and OD to be 65 ± 15 and 27 ± 5 kJ mol^{-1}, respectively, listed in Table I. The vibrational energy of OH is larger than that of OD; in contrast, the rotational energy of OD is greater than that of OH.

C. Potential-energy surface and branching of the O(^{1}D) + CH_3OH reaction

A simplified figure showing only the important reaction paths that produce OH and H is shown in Fig. 7. A more complete scheme of PES including other product channels is available in Fig. S-2 of the supplementary material.[56] The O(^{1}D) + CH_3OH reaction is initiated according to two mechanisms – insertion and abstraction. The insertion process can proceed via two paths: into a C−H bond to form *trans*-$HOCH_2OH$ with exothermicity of 634 kJ mol^{-1} and into the O−H bond via the $CH_3O(O)H$ association complex lying 190 kJ mol^{-1} below the reactants, to give rise to CH_3OOH with the total exothermicity of 373 kJ mol^{-1} via a small insertion barrier of 20 kJ mol^{-1} (TS1/2s in Fig. 7). One of the MEP curves for the C−H insertion reaction is shown in Fig. S-3 of the supplementary material.[56] *Trans*-$HOCH_2OH$ can isomerize to *cis*-$HOCH_2OH$ with a barrier ∼13 kJ mol^{-1}. Both energized *trans*-$HOCH_2OH$ and CH_3OOH can further decompose to form H, OH, and H_2O via various channels. The direct paths for H abstraction can proceed via two channels: attacking the CH_3 moiety to form CH_2OH + OH (H_C-abstraction) or attacking the OH moiety to form CH_3O + OH (H_O-abstraction); both abstraction reactions proceed via shallow pre-reaction complexes (LMa and LMb) and transition-states (TSa and TSb) that have energy within 1 kJ mol^{-1} of the reactants (see Fig. 7). The structures of $CH_3O(O)H$, CH_3OOH, $HOCH_2OH$, and related transition states, predicted with the B3LYP//aug-cc-pVTZ method, are shown in Fig. 8.

The production of OH and OD in the reaction O(^{1}D) + CH_3OD was investigated for the following dominant channels:

$$O(^1D) + CH_3OD \rightarrow HOCH_2OD^* \text{ (C−H insertion)}, \quad \text{(R1)}$$

$$HOCH_2OD^* \rightarrow CH_2OD + OH \text{ (fission of new C−O bond)}, \quad \text{(R2)}$$

$$\rightarrow CH_2OH + OD \text{ (fission of old C−O bond)}, \quad \text{(R3)}$$

$$O(^1D) + CH_3OD \rightarrow CH_3OOD^* \text{ (O−D insertion)}, \quad \text{(R4)}$$

$$CH_3OOD^* \rightarrow CH_3O + OD \text{ (fission of O−O bond)}, \quad \text{(R5)}$$

$$O(^1D) + CH_3OD \rightarrow CH_2OD + OH \text{ (H_C-abstraction)}, \quad \text{(R6)}$$

$$O(^1D) + CH_3OD \rightarrow CH_3O + OD \text{ (D_O-abstraction)}. \quad \text{(R7)}$$

A more complete mechanism including channels for production of HOD, DOD, and HOH from decomposition of $HOCH_2OD$* is available in the supplementary material.[56]

For the reaction of O(^{1}D) with CH_3OH at room temperature, the predicted total rate coefficient, 4.8

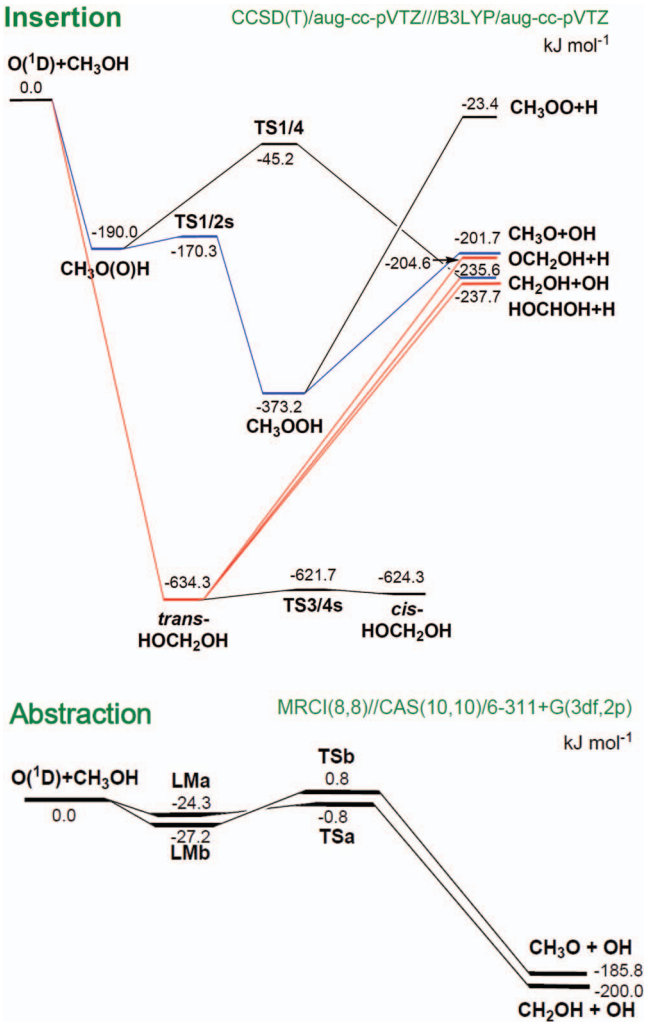

FIG. 7. Simplified potential-energy scheme for production of OH and H in the reaction $O(^1D) + CH_3OH$ computed with the CCSD(T)//B3LYP/aug-cc-pVTZ method. TS indicate transition states. Energy is in kJ mol^{-1}.

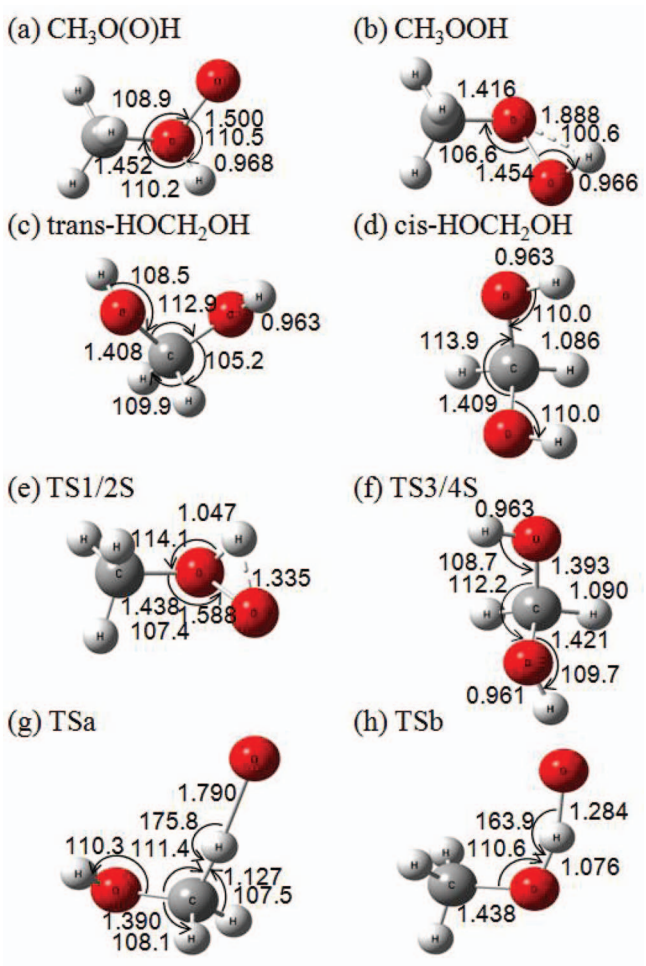

FIG. 8. Geometry of $CH_3O(O)H$, *trans*-$HOCH_2OH$, *cis*-$HOCH_2OH$, CH_3OOH and transition states TS1/2S, TS3/4S, TSa and TSb predicted with the B3LYP/aug-cc-pVTZ method. Bond lengths are in Å and bond angles are in deg.

$\times 10^{-10}$ cm^3 molecule^{-1} s^{-1}, is in agreement with the experimental value of $(5.1 \pm 0.1) \times 10^{-10}$ cm^3 molecule^{-1} s^{-1}.[19] About 88% of the reaction occurs by C−H insertion, 11% by O−H insertion, and the rest by direct abstraction from a C−H bond; the negligible contribution from abstraction from the O−H bond is expected according to the predicted potential energy profiles presented in Fig. 7. For the direct abstraction processes, the effect of the multiple reflections[57] above the pre-reaction complexes LMa and LMb have been included; the effect of the reflections might reduce predicted rate coefficients by as much as a factor of 2 at $T < 200$ K (depending on the temperature) and have a negligible effect above 500 K. The abstraction channels are unimportant because they have tight transition states, TSa and TSb, with the energies of −0.8 and 0.8 kJ mol^{-1}, respectively, relative to reactants, whereas the two insertion channels dominate because they are barrierless with less restriction on the configuration of the collisions. At temperatures below 1000 K, the total rate coefficients and the OH product branching ratio were found to be weakly dependent on temperature and independent of pressure below 10 atm because of the large excess energy carried by the insertion products and the small molecular size involved.

For the reaction of $O(^1D) + CD_3OH$, the following paths for production of OH and OD are possible:

$$O(^1D) + CD_3OH \rightarrow DOCD_2OH^* \text{ (C−D insertion)}, \quad \text{(R8)}$$

$$DOCD_2OH^* \rightarrow CD_2OH + OD \text{ (fission of new C−O bond)}, \quad \text{(R9)}$$

$$\rightarrow CD_2OD + OH \text{ (fission of old C−O bond)}, \quad \text{(R10)}$$

$$O(^1D) + CD_3OH \rightarrow CD_3OOH^* \text{ (O−H insertion)}, \quad \text{(R11)}$$

$$CD_3OOH^* \rightarrow CD_3O + OH \text{ (fission of O−O bond)}, \quad \text{(R12)}$$

$$O(^1D) + CD_3OH \rightarrow CD_2OH + OD \ (D_C\text{-abstraction}), \quad \text{(R13)}$$

$$O(^1D) + CD_3OH \rightarrow CD_3O + OH \ (H_O\text{-abstraction}). \quad \text{(R14)}$$

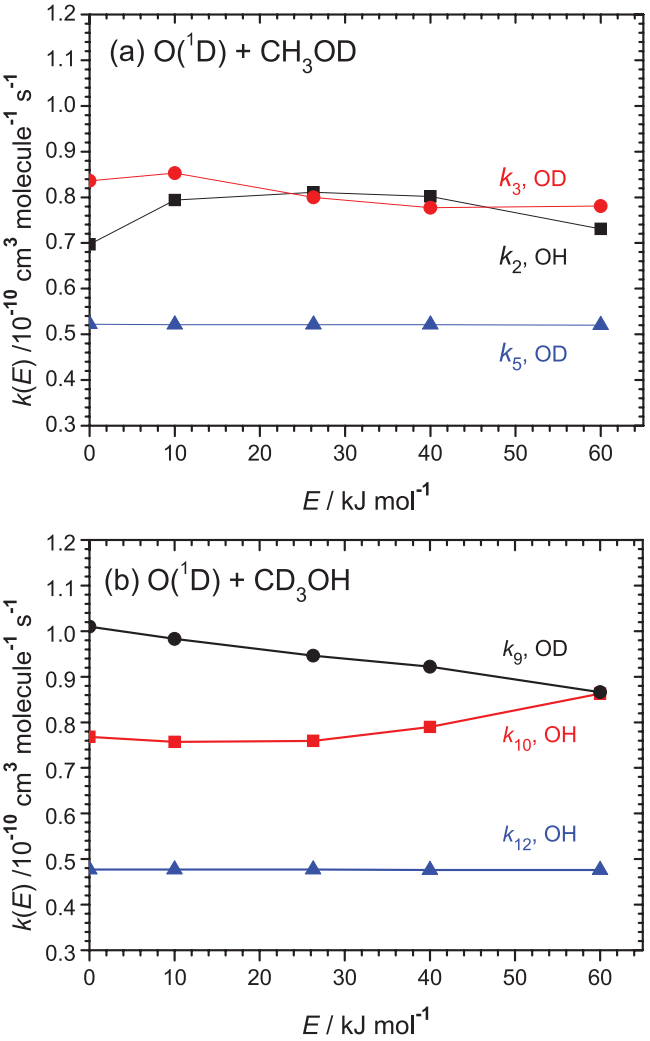

FIG. 9. Predicted microcanonical rate coefficients for reactions $O(^1D) + CH_3OD$ (a) and $O(^1D) + CD_3OH$ (b) as a function of excess energy relative to reactants.

The effect of isotopic substitution on the formation of various products can be readily evaluated with separate calculations on the system's vibrational frequencies and moments of inertia based on the predicted PES. The predicted individual rate coefficients for OH and OD production at room temperature from the $O(^1D)$ reactions with CH_3OD and CD_3OH as a function of the kinetic energy are presented in Figs. 9(a) and 9(b), respectively. The initial average kinetic energy of $O(^1D)$ that is produced upon photolysis of O_3 at 248 nm was determined to be 36 kJ mol^{-1} in the laboratory coordinates.[58] In the center-of-mass coordinates of the collision of $O(^1D)$ with CH_3OD or CD_3OH, the kinetic energy is 25.5 or 25.9 kJ mol^{-1}, respectively.

The predicted results reveal one major OH (k_2) and two OD (k_3 and k_5) production channels in the $O(^1D) + CH_3OD$ reaction and one OD (k_9) and two OH (k_{10} and k_{12}) production channels in the $O(^1D) + CD_3OH$ reaction. For $O(^1D) + CH_3OD$, the rate coefficient for OH/OD production is dominated by k_2 and k_3 (insertion of O into the C−H bond followed by rupture of the new and old C−O bonds); k_3 is slightly greater than k_2 at low collision energies but they become comparable ($\sim 8.0 \times 10^{-11}$ cm^3 molecule^{-1} s^{-1}) at collision energies greater than 26 kJ. The rate coefficients k_3 and k_2 remain nearly constant for higher energies because of the large exothermicity of these reaction channels. The bimolecular rate coefficient k_5 (insertion of O into the O−D bond, followed by rupture of the O−O bond) remains nearly constant (5.2×10^{-11} cm^3 molecule^{-1} s^{-1}) throughout the energy range 0−60 kJ mol^{-1} and is ~0.65 times k_2 and k_3 for energies at 26 kJ mol^{-1}; reaction (R5) is the only dominant channel from the O−H insertion. For $O(^1D) + CD_3OH$, the rate coefficient for production of OH/OD is also dominated by k_9 and k_{10} (insertion of O into the C−D bond before fission of the OH and OD groups); k_9 is about 1.3 times k_{10} at low collision energy but become comparable at 60 kJ mol^{-1}. k_{12} (insertion of O into the O−H bond, followed by rupture of the OH group), similar to k_5, remains nearly constant (4.8×10^{-11} cm^3 molecule^{-1} s^{-1}) in the 0−60 kJ energy range; it is about 63% of k_{10} and 50% that of k_9 at 26 kJ mol^{-1}.

The ratios of k_{OH}/k_{OD} from the reactions $O(^1D) + CH_3OD/CD_3OH$, shown in Fig. 10, were calculated according to these rate coefficients. For the reaction $O(^1D) + CH_3OD$, $k_{OH}/k_{OD} = k_2/(k_3 + k_5) \cong 0.51$, whereas for the reaction $O(^1D) + CD_3OH$, $k_{OH}/k_{OD} = (k_{10} + k_{12})/k_9 \cong 1.23$ at $E = 0$ kJ mol^{-1}. These ratios increase gradually and become 0.61 and 1.31, respectively, at 26 kJ mol^{-1}, in satisfactory agreement with the experimental results of 0.59 ± 0.14 and 1.56 ± 0.36.

Similarly, we calculated also the ratios of k_H/k_D for the reaction $O(^1D) + CH_3OD$ according to the reactions

$$HOCH_2OD^* \rightarrow OCH_2OD + H \text{ (fission of new O−H bond)}, \quad \text{(R15)}$$

$$\rightarrow OCH_2OH + D \text{ (fission of old O−D bond)}, \quad \text{(R16)}$$

$$\rightarrow HOCHOD + H \text{ (fission of C−H bond)}, \quad \text{(R17)}$$

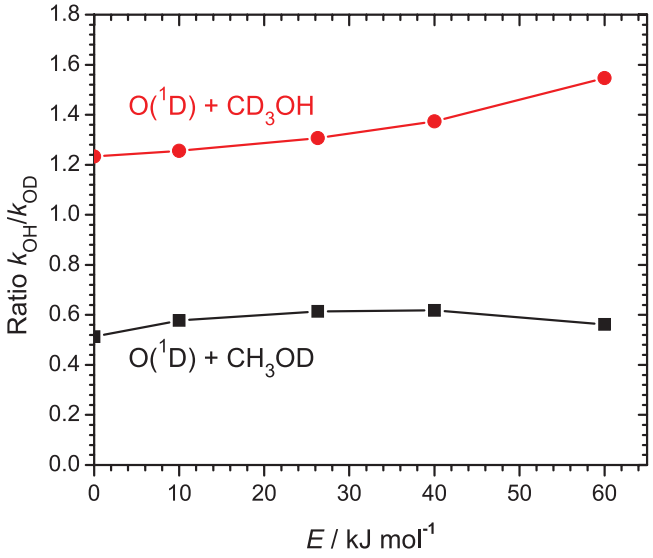

FIG. 10. Predicted k_{OH}/k_{OD} for reactions $O(^1D) + CH_3OD$ and $O(^1D) + CD_3OH$ as a function of excess energy relative to reactants.

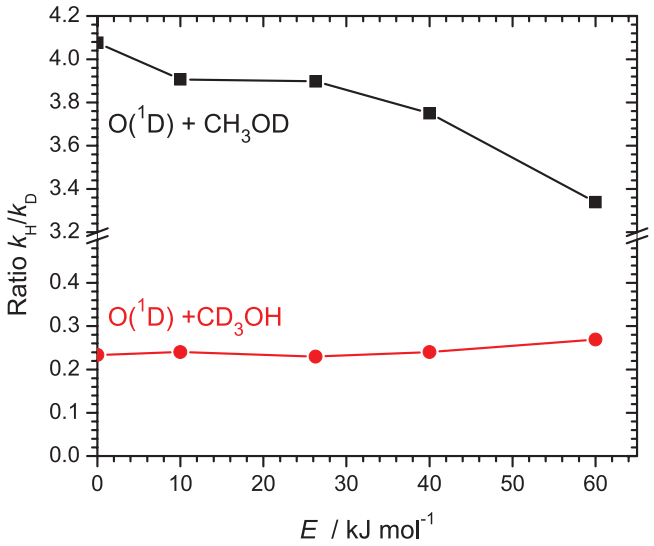

FIG. 11. Predicted ratios k_H/k_D for reactions $O(^1D)$ + CH_3OD and $O(^1D)$ + CD_3OH as a function of excess energy relative to reactants.

and for the reaction $O(^1D)$ + CD_3OH according to the reactions

$$DOCD_2OH^* \rightarrow OCD_2OH + D \text{ (fission of new O−D bond)}, \quad \text{(R18)}$$

$$\rightarrow OCD_2OD + H \text{ (fission of old O−H bond)}, \quad \text{(R19)}$$

$$\rightarrow DOCDOH + D \text{ (fission of C−D bond)}. \quad \text{(R20)}$$

The O−H insertion product, CH_3OOH^*, which accounts for only 11% of the insertion/decomposition processes as aforementioned, decomposes mainly by breaking its weak O−O bond to form OH radical. As shown in Fig. 11, the ratio of $k_H/k_D = (k_{15} + 2k_{17})/k_{16}$ predicted with RRKM calculations for the reaction $O(^1D)$ + CH_3OD decreases from 4.1 to 3.3 as the excess energy increases from 0 to 60 kJ mol^{-1}, whereas the ratio of $k_H/k_D = k_{19}/(k_{18} + 2k_{20})$ for the reaction $O(^1D)$ + CD_3OH increases from 0.23 to 0.27. These values are insensitive to the temperature or the kinetic energy carried by the O atom, again attributable to the large amount of energy carried by the insertion products. At the collision energy of 26 kJ mol^{-1}, the ratios are 3.9 for $O(^1D)$ + CH_3OD and 0.23 for $O(^1D)$ + CD_3OH.

D. Mechanism for formation of OH and OD

According to our theoretical calculations, the abstraction channels are unimportant. For the insertion channels, two intermediates are possible: $HOCH_2OH$ from insertion into the C−H bond and CH_3OOH from insertion into the O−H bond. The formation of $HOCH_2OH$ is supported by the observation of this species in an UV-irradiated Ar matrix containing O_3 and CH_3OH.[59] The CH_3OOH intermediate has not been identified directly.

The observation of bimodal rotational distributions for OD and Boltzmann distribution for OH produced from the $O(^1D)$ + CH_3OD reaction indicates that the reaction might proceed via three major channels. This experimental observation is consistent with the predicted mechanism that has a single channel for formation of OH, reaction (R2), and two channels for formation of OD, reactions (R3) and (R5). Similarly, the observation of a Boltzmann rotational distribution for OD and a bimodal rotational distribution for OH in the reaction $O(^1D)$ + CD_3OH is consistent with the predicted mechanism that has a single channel for formation of OD, reaction (R9), and two channels for formation of OH, reactions (R10) and (R12).

For the reaction $O(^1D)$ + CH_3OD, the observed OH has greater vibrational energy than OD, whereas the additional rotational component of OD has greater rotational excitation than OH and the low-J component of OD. Similarly, for the reaction $O(^1D)$ + CD_3OH, the observed OD has greater vibrational energy than OH, whereas the additional rotational component of OH has greater rotational excitation than OD and the low-J component of OH. These results indicate that the fission of the O−O bond of CH_3OOD and CD_3OOH, reactions (R5) and (R12), produces the hydroxyl radical with smaller vibrational energy but greater rotational energy. The bond angle∠HOO in CH_3OOH is 100.6°, whereas the bond angle∠COH in *trans*-$HOCH_2OH$ is 108.5° (Fig. 8). Considering the torque angle during bond fission, one would expect that the OH produced from CH_3OOH receives greater rotational excitation than that from $HOCH_2OH$, consistent with experimental observations.

Regarding the vibrational excitation of the hydroxyl radical product, as described above, we observed that the hydroxyl radical produced from the methyl moiety has vibrational excitation greater than that from the hydroxyl moiety of methanol. In the case of $O(^1D)$ + CD_3OH, the vibrational energy of OD is about 20% of the reaction energy, which is more than the statistical partitioning if one considers the complexity of the co-product CD_2OH. This fact indicates that the reaction does not proceed through a long-lived intermediate. There are two possibilities for the observed extensive vibrational excitation for the hydroxyl radical produced from the methyl moiety. One mechanism is that $O(^1D)$ abstracts directly one H atom from the methyl group, as was observed in the reaction $O(^1D)$ + CH_4.[1] In the reaction $O(^1D)$ + CH_4 in crossed molecular beams, a large proportion of the OH product scatters in the forward direction because of direct abstraction, and OH had much more vibrational than rotational excitation. The second mechanism is that when the reacting O atom, indicated as O*, inserts into the H−C bond of the CH_3 moiety, the newly formed HO*−C bond breaks more rapidly than the original C−OH bond; that is, $k_2 > k_3$ and $k_9 > k_{10}$. This condition implies that the lifetime of a portion of the HO^*CH_2OH intermediate is too small for complete IVR, consistent with the conclusion derived from comparison of observed and calculated [OH]/[OD], to be discussed later. The reaction energy thus becomes localized near the newly formed bond upon insertion of $O(^1D)$ into the H−C bond, and highly vibrationally excited O*H is produced quickly. Some HO^*CH_2OH survives to allow energy redistribution before the fission of the C−OH bond to form less vibrationally excited OH. Both elimination channels from $HOCH_2OH$ likely produce OH with little rotational excitation because of a smaller torque angle as indicated above.

A similar non-equilibrium reaction of $O(^1D)$ was reported for the reaction $^{16}O(^1D) + H_2{}^{18}O \rightarrow {}^{16}OH + {}^{18}OH$ in which ^{16}OH is from the newly formed moiety, whereas ^{18}OH is a part of the original reactant.[60–66] The product ^{16}OH was found to be highly vibrationally excited, whereas ^{18}OH was vibrationally much cooler. This condition indicates that $^{16}O(^1D)$ reacts quickly with H in $H_2{}^{18}O$ to form ^{16}OH, with the remaining product ^{18}OH being a spectator. Our observation of vibrationally excited OH (OD) from the channel associated with the rupture of the new C−O bond in $HOCH_2OD$ ($DOCD_2OH$) is consistent with the results of $O(^1D) + H_2O$.

In the reaction of $O(^1D) + CD_3OH$, the observed ratio is $[OH]/[OD] \cong 1.56 \pm 0.36$, whereas in the reaction of $O(^1D) + CH_3OD$, the product ratio is $[OH]/[OD] \cong 0.59 \pm 0.14$. This indicates that the hydroxyl radical products derive their H or D atoms preferably from the hydroxyl site of methanol. However, because insertion of the O atom into the C−H bond might be followed by fragmentation of the original hydroxyl moiety, listed as reactions (R3) and (R10), these product ratios do not necessarily indicate the preference of the reaction of $O(^1D)$ with the hydroxyl moiety over the methyl moiety of methanol. In fact, the calculations predicted that about 88% of the reaction occurs by C−H insertion and 11% by O−H insertion.

In the reaction of $O(^1D) + CH_3OD$, the ratio of [OH]/[OD] depends mainly on $k_{OH}/k_{OD} = k_2/(k_3 + k_5)$ according to reactions (R1)−(R5) listed in Sec. IV C. In the reaction of $O(^1D) + CD_3OH$, the ratio of [OH]/[OD] depends on $k_{OH}/k_{OD} = (k_{10} + k_{12})/k_9$. If one ignores the kinetic isotopic effects, $k_9 \cong k_2$ for fission of the newly formed C−O bond, $k_{10} \cong k_3$ for fission of the old C−O bond, and $k_{12} \cong k_5$ for fission of the O−O bond. Hence, the ratio of [OH]/[OD] for the reaction $O(^1D) + CH_3OD$ is expected to be approximately the inverse of the [OH]/[OD] ratio for the reaction $O(^1D) + CD_3OH$. Our observed values of $[OH]/[OD] = 0.59$ for the reaction $O(^1D) + CH_3OD$ and $[OH]/[OD] = 1.56$ for the reaction $O(^1D) + CD_3OH$ are consistent with this scheme; these observed ratios indicate that $(k_3 + k_5) > k_2$ and $(k_{10} + k_{12}) > k_9$. Without considering the kinetic isotope effect, one would expect that $k_2 \cong k_3$ and $k_9 \cong k_{10}$, if the IVR is much more rapid than bond fission. If the bond rupture is more rapid than energy randomization, one would expect that k_2/k_3 and k_9/k_{10} becomes greater than 1.

At the center-of-mass collision energy of 26 kJ mol^{-1} for $O(^1D)$ with methanol, the ratio of $[OH]/[OD] = (k_{10} + k_{12})/k_9 = 1.31$, predicted for $O(^1D) + CD_3OH$ such that energy is randomized before bond rupture, is slightly smaller than our experimental value of 1.56 ± 0.36; the value of $[OH]/[OD] = 1/(0.4 \pm 0.2)$ reported by Goldstein and Wiesenfeld has a large error.[18] These results are consistent with the condition in which the breaking of the newly formed C−OD bond is more rapid than the breaking of the old C−OH bond in $DOCD_2OH$ such that observed k_9/k_{10} is greater than prediction. Similarly, the ratio of $[OH]/[OD] = k_2/(k_3 + k_5)$ is predicted to be 0.61 for $O(^1D) + CH_3OD$. This predicted value is in close agreement with our experimental value of 0.59 ± 0.14; both are greater than the value of 0.43 reported by Goldstein and Wiesenfeld.[18] Considering possible errors, this result is not inconsistent with the condition in which IVR is slower than the bond rupture such that the breaking of the newly formed C−OH bond is more rapid than the breaking of the old C−OD bond in $HOCH_2OD$, i.e., observed k_2/k_3 is greater than prediction; the slower IVR was indicated by the observation of vibrationally excited OH, as discussed above.

The reported experimental value of $[H]/[D] = 7.1 \pm 0.8$ for $O(^1D) + CH_3OD$ at room temperature[19] is much larger than the value of $k_H/k_D = (k_{15} + 2k_{17})/k_{16} = 3.90$ predicted according to the microcanonical rate coefficients at $E = 26$ kJ mol^{-1}. On the other hand, for $O(^1D) + CD_3OH$, the observed ratio of $[H]/[D] = 0.26 \pm 0.03$ (Ref. 19) is in agreement with the value of $k_H/k_D = k_{19}/(k_{18} + 2k_{20}) = 0.23$ predicted according to the microcanonical rate coefficients insensitive to the collision energies from 0−60 kJ mol^{-1}. The much larger discrepancy might indicate that the rate of bond rupture for formation of H or D atoms is much more rapid than IVR. The IVR rates of the skeletal modes involving the O−H bond are much smaller than those of the C−O bonds; the former are associated with formation of H, whereas the latter are with formation of OH. Furthermore, part of the discrepancy might be accounted for by secondary decomposition of OCH_2OD, $HOCH_2O$, and HOCHOD products.

According to our calculated rate coefficients, the quantum yields for production of H (and D) and OH (and OD) are 0.158 and 0.548 for the reaction $O(^1D) + CH_3OD$ and 0.186 and 0.540 for the reaction $O(^1D) + CD_3OH$. Matsumi *et al.* reported a quantum yield of 0.18 for production of H atom in the reaction of $O(^1D) + CH_3OH$,[19] consistent with our calculation.

V. CONCLUSION

By monitoring the IR emission of products OH and OD with a step-scan Fourier-transform infrared spectrometer, we investigated the reactions $O(^1D) + CD_3OH/CH_3OD$. For the reaction of $O(^1D) + CD_3OH$, the nascent average rotational energies are estimated to be 6 ± 2 and 12 ± 4 kJ mol^{-1} and the average vibrational energies are 43 ± 8 and 28 ± 6 kJ mol^{-1} for OD and OH, respectively. Product OD is vibrationally more excited than OH, whereas OH shows a bimodal rotational distribution with the additional component having greater rotational excitation than OD. The product ratio [OH]/[OD] is estimated to be $61/39 = 1.56$.

For the reaction $O(^1D) + CH_3OD$, the nascent rotational energies are estimated to be 6 ± 2 and 10 ± 3 kJ mol^{-1} and the average vibrational energies are 65 ± 15 and 27 ± 5 kJ mol^{-1} for OH and OD, respectively. Product OH is vibrationally more excited than OD, whereas OD shows a bimodal rotational distribution with the additional component having greater rotational excitation than OH. The product ratio [OH]/[OD] was estimated to be $37/63 = 0.59$, nearly the inverse of that of the reaction $O(^1D) + CD_3OH$.

The experimental observations are explicable according to a mechanism of $O(^1D) + CH_3OD$ involving two insertion intermediates, $HOCH_2OD$ and CH_3OOD, and three major decomposition channels, reactions (R2), (R3), and (R5). Insertion of $O(^1D)$ into the C−H bond to form $HOCH_2OD$ followed by fission of the newly formed HO−C bond, reaction (R2), produces vibrationally more excited OH because

of incomplete IVR, whereas fission of the old C−OD bond in $HOCH_2OD$, reaction (R3), produces OD with less vibrational excitation. Insertion of $O(^1D)$ into the O−D bond to form CH_3COOD followed by fission of the O−O bond, reaction (R5), produced OD with greater rotational excitation, likely due to a large torque angle during dissociation. A similar mechanism applies for $O(^1D) + CD_3OH$: two insertion intermediates, $DOCD_2OH$ and CD_3OOH, and three decomposition channels, reactions (R9), (R10), and (R12), are involved.

For $O(^1D) + CH_3OD$, the observed ratio of [OH]/[OD] $= 0.59 \pm 0.14$ is close to the value of 0.61 predicted according to microcanonical rate coefficients. For $O(^1D) + CD_3OH$, the observed ratio of [OH]/[OD] $= 1.56 \pm 0.36$ is also close to the predicted value of 1.31. The small deviations are likely due to incomplete IVR.

For $O(^1D) + CD_3OH$, the observed ratio of [H]/[D] $= 0.26 \pm 0.03$ is close to the predicted value of 0.23. For $O(^1D) + CH_3OD$, the reported observed ratio of [H]/[D] $= 7.1 \pm 0.8$ is much larger than the value of 3.90 predicted according to microcanonical rate coefficients. The much larger discrepancy might indicate that the rate of bond rupture for formation of H or D atoms is much more rapid than IVR. Part of the discrepancy might be accounted for by secondary decomposition reactions of OCH_2OD, $HOCH_2O$, and HOCHOD which were assumed to be negligible in our prediction.

It should be emphasized that even though the observed [OH]/[OD] indicates a preference of formation of OH from the hydroxyl moiety over the methyl moiety of CH_3OH, it is not in conflict with the theoretical prediction that $O(^1D)$ prefers to attack the methyl moiety of CH_3OH. This is partly because, upon insertion of $O(^1D)$ to a C−H bond to form $HOCH_2OH^*$, subsequent dissociation occurs for both the newly formed OH and the original OH group, and partly because this inserted intermediate $HOCH_2OH^*$ can also decompose to form H and H_2O, whereas the decomposition of CH_3OOH, produced from insertion of $O(^1D)$ into the O−H bond, produces mainly $CH_3O + OH$.

ACKNOWLEDGMENTS

National Science Council of Taiwan (Grant No. NSC100-2745-M009-001-ASP) and the Ministry of Education, Taiwan ("Aim for the Top University Plan" of National Chiao Tung University) supported this work. The National Center for High-Performance Computing provided computer time. M.C.L. acknowledges the support from National Science Council of Taiwan for the distinguished visiting professorship and Taiwan Semiconductor Manufacturing Co. for the TSMC distinguished professorship (2005–2011) at the National Chiao Tung University.

[1] X. Yang, Phys. Chem. Chem. Phys. **8**, 205 (2006), and references cited therein.
[2] A. C. Luntz, J. Chem. Phys. **73**, 1143 (1980).
[3] P. M. Aker, J. J. A. O'Brien, and J. J. Sloan, J. Chem. Phys. **84**, 745 (1986).
[4] S. G. Cheskis, A. A. Iogasen, P. V. Kulakov, I. Yu. Razuvaev, O. M. Sarkisov, and A. A. Titóv, Chem. Phys. Lett. **155**, 37 (1989).
[5] C. R. Park and J. R. Wiesenfeld, J. Chem. Phys. **95**, 8166 (1991).
[6] Y. Rudich, Y. Hurwitz, G. J. Frost, V. Vaida, and R. Naaman, J. Chem. Phys. **99**, 4500 (1993).
[7] S. Wada and K. Obi, J. Phys. Chem. A **102**, 3481 (1998).
[8] M. Gonzalez, M. P. Puyuelo, J. Hernando, R. Sayos, P. A. Enriquez, J. Guallar, and I. Banos, J. Phys. Chem. A **104**, 521 (2000).
[9] T. Suzuki and E. Hirota, J. Chem. Phys. **98**, 2387 (1993).
[10] R. Schott, J. Schluter, M. Olzmann, and K. Kleinermanns, J. Chem. Phys. **102**, 8371 (1995).
[11] A. H. H. Chang and S. H. Lin, Chem. Phys. Lett. **363**, 175 (2002).
[12] A. H. H. Chang and S. H. Lin, Chem. Phys. Lett. **384**, 229 (2004).
[13] C. C. Miller, R. D. van Zee, and J. C. Stephenson, J. Chem. Phys. **114**, 1214 (2001).
[14] H. Arai, S. Kato, and S. Kofda, J. Phys. Chem. A **98**, 12 (1994).
[15] M. Gonzalez, J. Hernando, I. Banos, and R. Sayos, J. Chem. Phys. **111**, 8913 (1999).
[16] J. Hernando, J. Millan, R. Sayos, and M. Gonzalez, J. Chem. Phys. **119**, 9504 (2003).
[17] M. Gonzalez, J. Hernando, I. Banos, and R. Sayos, J. Chem. Phys. **113**, 6748 (2000).
[18] N. Goldstein and J. R. Wiesenfeld, J. Chem. Phys. **78**, 6725 (1983).
[19] Y. Matsumi, Y. Inagaki, and M. Kawasaki, J. Phys. Chem. **98**, 3777 (1994).
[20] R. Atkinson, D. L. Baulch, R. A. Cox, R. F. Hampson, Jr., J. A. Kerr, M. J. Rossi, and J. J. Troe, Phys. Chem. Ref. Data **26**, 521 (1997).
[21] P.-S. Yeh, G.-H. Leu, Y.-P. Lee, and I.-C. Chen, J. Chem. Phys. **103**, 4879 (1995).
[22] S.-R. Lin and Y.-P. Lee, J. Chem. Phys. **111**, 9233 (1999).
[23] C.-Y. Wu, C.-Y. Chung, Y.-C. Lee, and Y.-P. Lee, J. Chem. Phys. **117**, 9785 (2002).
[24] S.-K. Yang, S.-Y. Liu, H.-F. Chen, and Y.-P. Lee, J. Chem. Phys. **123**, 224304 (2005).
[25] Y. Matsumi and M. Kawasaki, Chem. Rev. **103**, 4767 (2003).
[26] L. T. Molina and M. J. Molina, J. Geophys. Res. **91**, 14501, doi:10.1029/JD091iD13p14501 (1986).
[27] A. D. Becke, J. Chem. Phys. **98**, 5648 (1993).
[28] C. Lee, W. Yang, and R. G. Parr, Phys. Rev. B **37**, 785 (1988).
[29] T. H. Dunning, Jr., J. Chem. Phys. **90**, 1007 (1989).
[30] D. E. Woon and T. H. Dunning, Jr., J. Chem. Phys. **98**, 1358 (1993).
[31] J. A. Pople, M. Head-Gordon, and K. Raghavachari, J. Chem. Phys. **87**, 5968 (1987).
[32] G. E. Scuseria and H. F. Schaefer III, J. Chem. Phys. **90**, 3700 (1989).
[33] H.-J. Werner and P. J. Knowles, J. Chem. Phys. **82**, 5053 (1985).
[34] P. J. Knowles and H.-J. Werner, Chem. Phys. Lett. **115**, 259 (1985).
[35] C. Gonzalez and H. B. Schlegel, J. Chem. Phys. **90**, 2154 (1989).
[36] M. J. Frisch, G. W. Trucks, H. B. Schlegel *et al.*, GAUSSIAN 03, Revision C.01, Gaussian, Inc., Wallingford, CT, 2004.
[37] H.-J. Werner, P. J. Knowles, R. Lindh, F. R. Manby, M. Schütz *et al.*, MOLPRO, version 2009.1, a package of *ab initio* programs, 2009, see http://www.molpro.net.
[38] C. Eckart, Phys. Rev. **35**, 1303 (1930).
[39] D. M. Wardlaw and R. A. Marcus, Chem. Phys. Lett. **110**, 230 (1984).
[40] D. M. Wardlaw and R. A. Marcus, J. Chem. Phys. **83**, 3462 (1985).
[41] S. J. Klippenstein, J. Chem. Phys. **96**, 367 (1992).
[42] S. J. Klippenstein and R. A. Marcus, J. Chem. Phys. **87**, 3410 (1987).
[43] S. J. Klippenstein, A. F. Wagner, R. C. Dunbar, D. M. Wardlaw, and S. H. Robertson, VARIFLEX version 1.00, 1999.
[44] D. C. Astholz, J. Troe, and W. Wieters, J. Chem. Phys. **70**, 5107 (1979).
[45] J. A. Miller and S. J. Klippenstein, J. Phys. Chem. A **104**, 2061 (2000).
[46] F. M. Mourits and F. H. Rummens, Can. J. Chem. **55**, 3007 (1977).
[47] F. Melen, A. J. Sauval, N. Grevesse, C. B. Farmer, C. Servais, L. Delbouille, and D. Roland, J. Mol. Spectrosc. **174**, 490 (1995).
[48] M. C. Abrams, S. P. Davis, M. L. P. Rao, R. Engleman, Jr., and J. W. Brault, Astrophys. J., Suppl. **93**, 351 (1994).
[49] C. Amiot, J.-P. Mailard, and J. Chauville, J. Mol. Spectrosc. **87**, 196 (1981).
[50] T. Amano, J. Mol. Spectrosc. **103**, 436 (1984).
[51] M. C. Abrams, S. P. Davis, M. L. P. Rao, and R. Engelman, Jr., J. Mol. Spectrosc. **165**, 57 (1994).
[52] R. Herman and R. F. Wallis, J. Chem. Phys. **23**, 637 (1955).
[53] D. D. Nelson, Jr., A. Schiffman, D. J. Nesbitt, J. J. Orlando, and J. B. Burkholder, J. Chem. Phys. **93**, 7003 (1990).
[54] K. W. Holtzclow, J. C. Person, B. D. Green, and J. Quant, J. Quant. Spectrosc. Radiat. Transf. **49**, 223 (1993).
[55] D. D. Nelson, Jr., A. Schiffman, D. J. Nesbitt, and D. J. Yaron, J. Chem. Phys. **90**, 5443 (1989).

[56]See supplementary material at http://dx.doi.org/10.1063/1.4759619 for calculated Einstein *A* coefficients of OD, the A coefficient for Meinel band of OD, and a more complete PES and reaction mechanism for $O(^1D) + CH_3OH$.
[57]W. H. Miller, J. Chem. Phys. **65**, 2216 (1976).
[58]M.-A. Thelen, T. Gejo, J. A. Harrison, and J. R. Huber, J. Chem. Phys. **103**, 7946 (1995).
[59]C. Lugez, A. Schriver, R. Levant, and L. Shriver-Mazzuoli, Chem. Phys. **181**, 129 (1994).
[60]E. J. Comes, K. H. Gericke, and J. Manz, J. Chem. Phys. **75**, 2853 (1981).
[61]J. E. Butler, L. D. Talley, G. K. Smith, and M. C. Lin, J. Chem. Phys. **74**, 4501 (1981).
[62]K. H. Gericke, F. J. Comes, and R. D. Levine, J. Chem. Phys. **74**, 6106 (1981).
[63]C. B. Cleveland and J. R. Wiesenfeld, J. Chem. Phys. **96**, 248 (1992).
[64]D. G. Sauder, J. C. Stephenson, D. S. King, and M. P. Casassa, J. Chem. Phys. **97**, 952 (1992).
[65]D. S. King, D. G. Sauder, and M. P. Casassa, J. Chem. Phys. **97**, 5919 (1992).
[66]N. Tanaka, M. Takayanagi, and I. Hanazaki, Chem. Phys. Lett. **254**, 40 (1996).